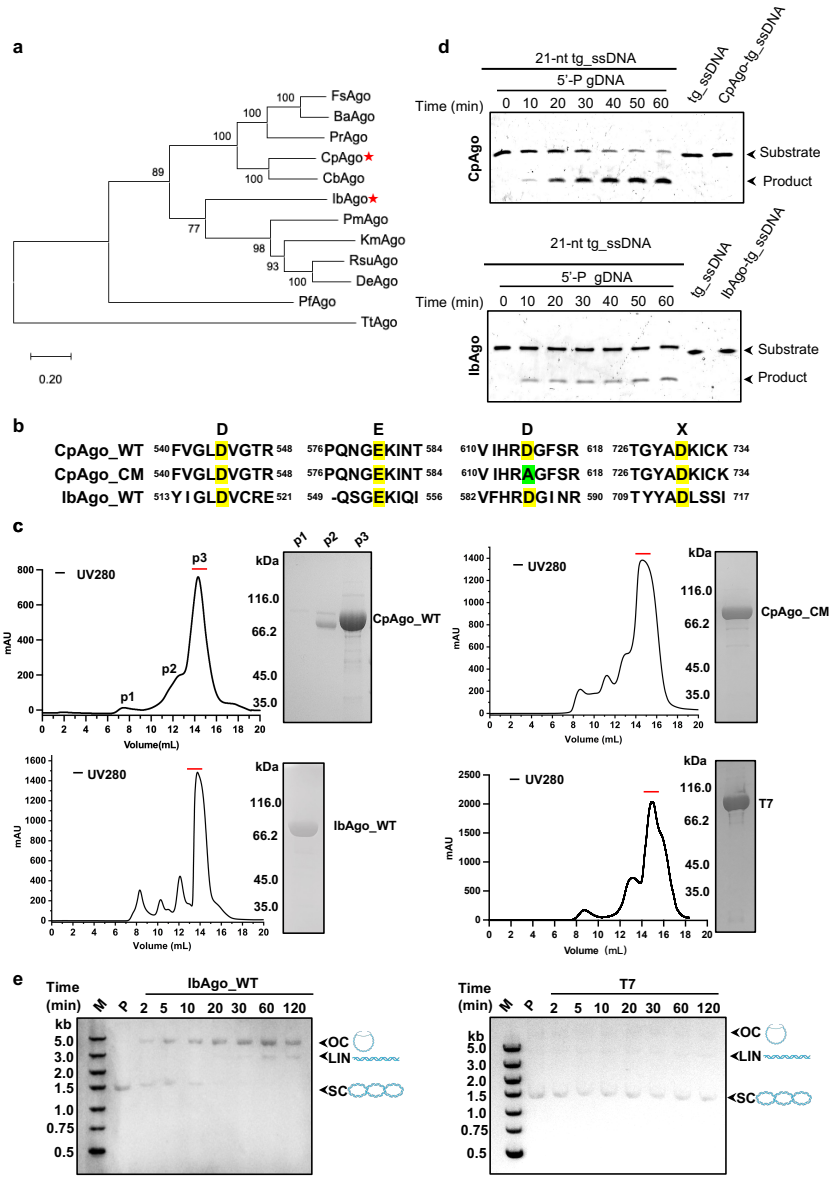

Supplementary Figure 1: CpAgo exhibits guide-independent and DNA-guided activity at 37°C.

a Neighbor-joining phylogenetic tree analysis of CpAgo based on amino acid sequences through MEGA11 software. Bootstrap values at the nodes were determined from 1,000 resampled data sets. The scale bar was utilized to indicate the evolutionary distance between species.

b Multiple sequence alignment of the partial PIWI domain from CpAgo and its catalytic mutant (D614A, CpAgo_CM) with IbAgo.

c Size-exclusion chromatography analysis of CpAgo, CpAgo_CM, IbAgo, and T7 RNA polymerase.

d Guide-dependent cleavage activity assay results for CpAgo and IbAgo. The assays were performed at 37°C in time gradient.

e Specificity controls for guide-independent plasmid degradation. Left: IbAgo exhibits weak guide-independent plasmid degradation over time. Right: T7 RNA polymerase purified using the same protocol shows no detectable plasmid degradation, ruling out nuclease contamination. OC, open circular; LIN, linear; SC, supercoiled.

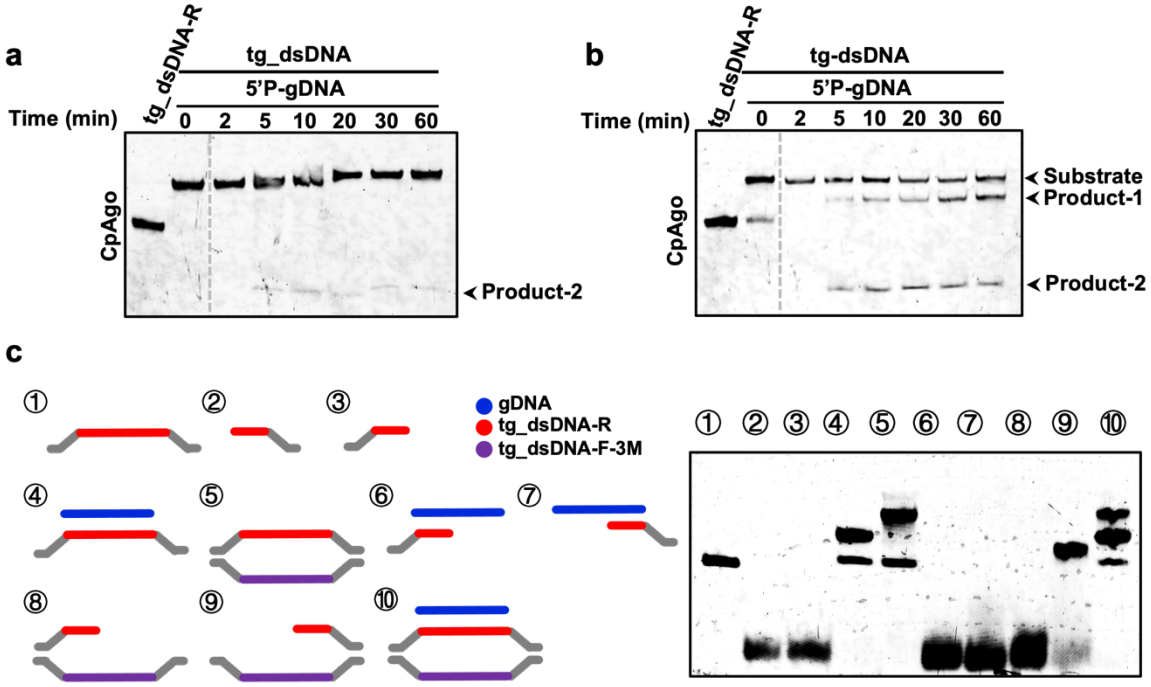

Supplementary Figure 2: CpAgo cleaves the partially unwound dsDNA.

a The cleavage assay of CpAgo with fully annealed dsDNA. The fully annealed dsDNA was prepared using gradient annealing.

b The cleavage assay of CpAgo with partially unwound dsDNA. The partially unwound dsDNA was prepared by heating at 95°C for 5 min, followed by cooling to room temperature for 20 min.

c Native PAGE assay showing the location of different annealing products among gDNA and tg_dsDNAs.

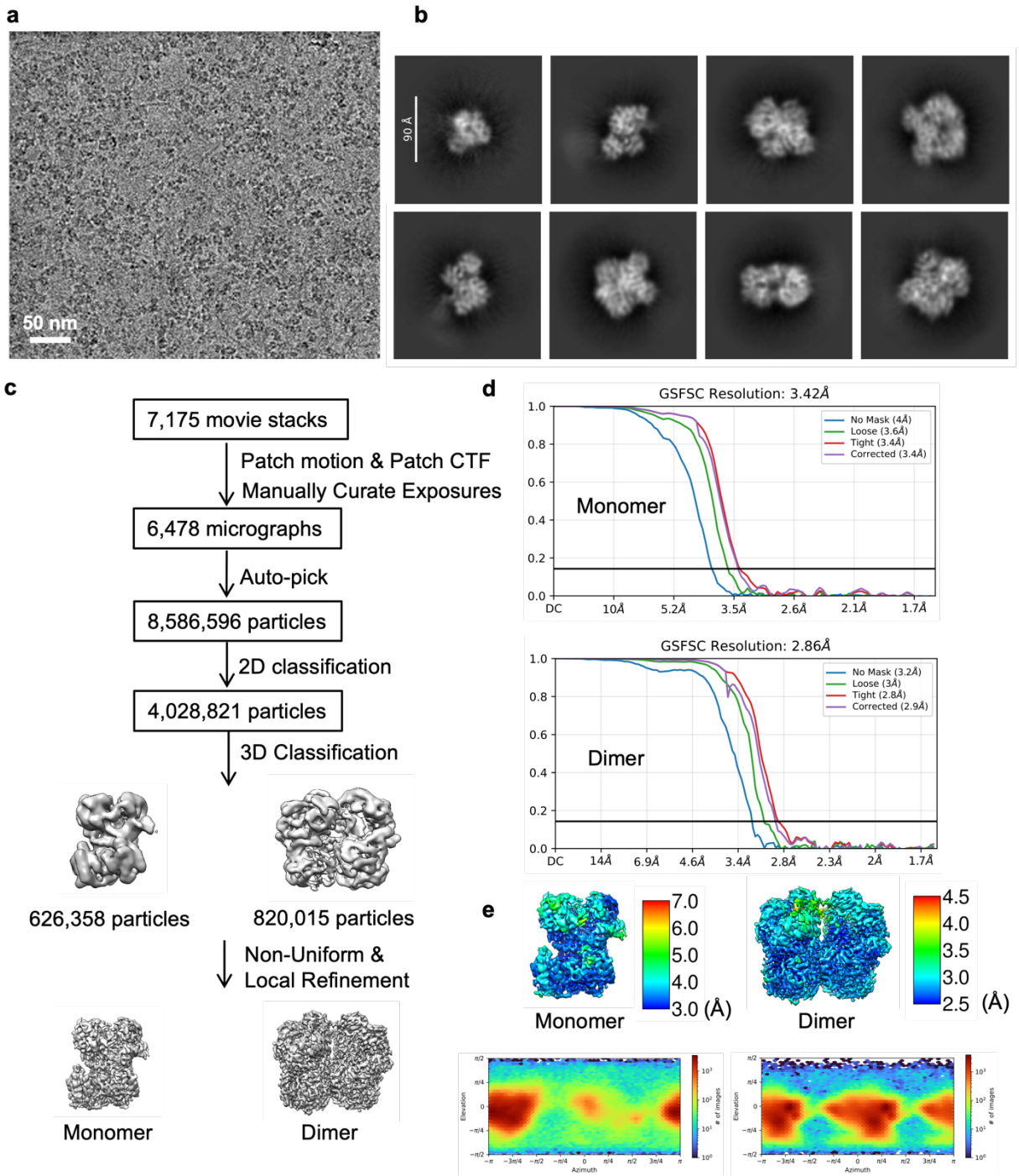

Supplementary Figure 3: Single-particle cryo-EM analysis of the CpAgo-gDNA-tg_dsDNA complex.

a Representative motion-corrected cryo-EM micrograph.

b Reference-free 2D class averages.

c Workflow of the data processing.

d Gold standard FSC plots for the 3D reconstructions, calculated in cryoSPARC.

e Resolution maps and euler angle distribution of the particle images for the final 3D reconstructions.

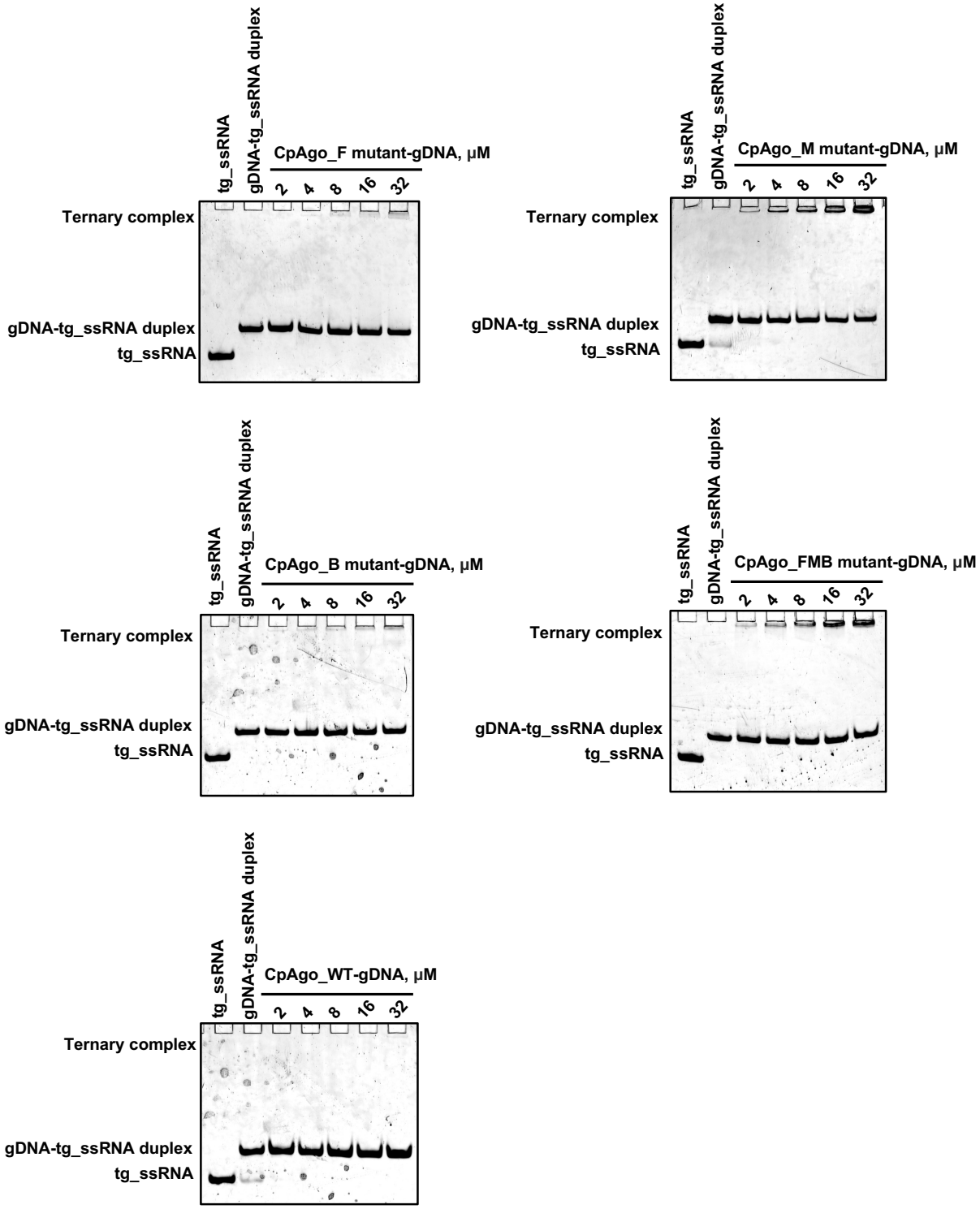

Supplementary Figure 4: EMSA analysis of CpAgo and PAZ pocket mutants binding to ssDNA substrates. EMSA was performed using 2 μM 5′-FAM-labeled 29-nt tg_ssDNA incubated with increasing concentrations (2, 4, 8, 16, 32 μM) of CpAgo-gDNA complexes at 37°C for 30 min. WT and four PAZ pocket charge-reversal mutants (F, M, B, and FMB) were assessed. Shifted bands indicate formation of ternary complexes.

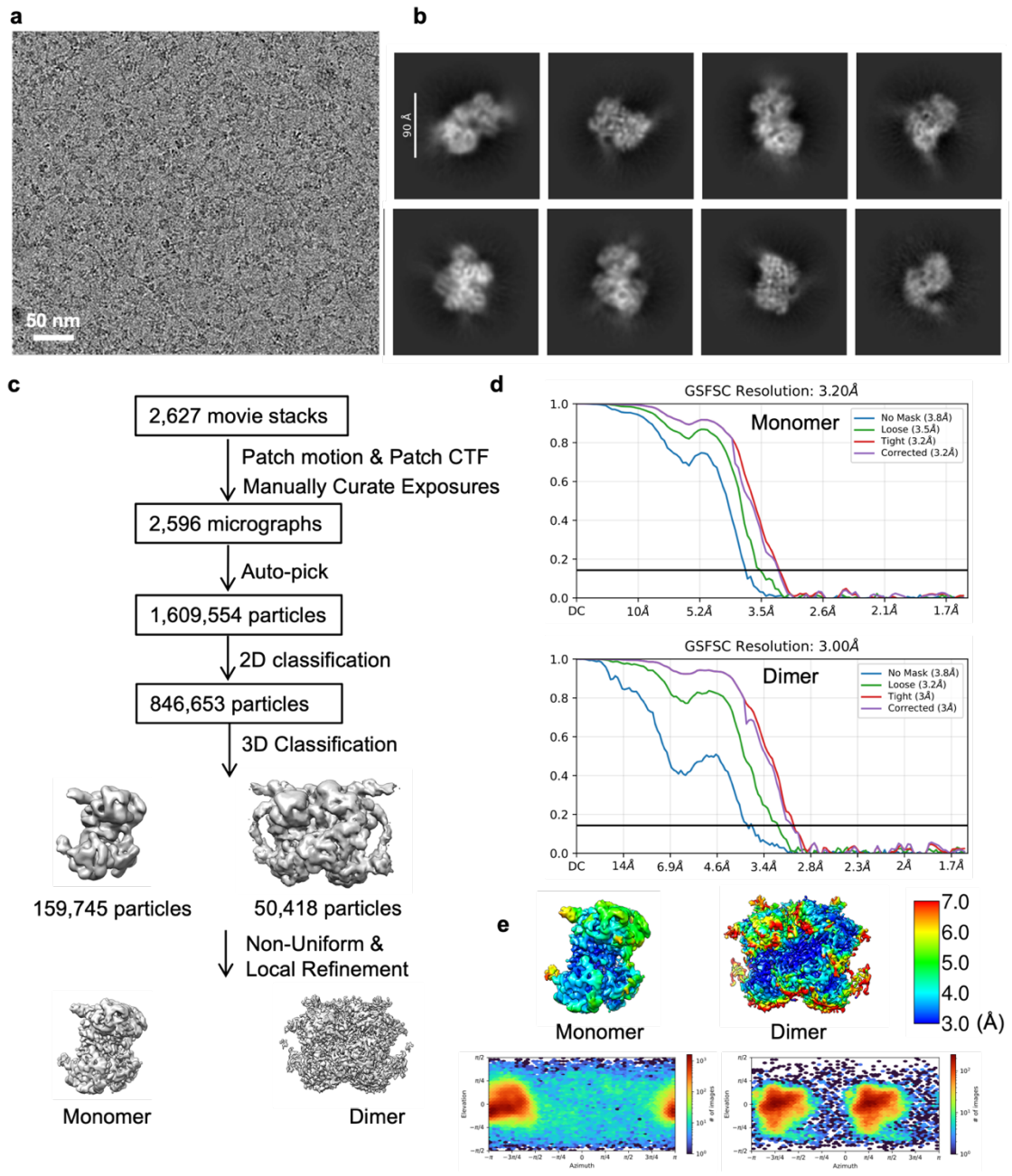

Supplementary Figure 5: Single-particle cryo-EM analysis of the CpAgo-gDNA-tg_bubble_dsDNA complex.

a Representative motion-corrected cryo-EM micrograph.

b Reference-free 2D class averages.

c Workflow of the data processing.

d Gold standard FSC plots for the 3D reconstructions, calculated in cryoSPARC.

e Resolution maps and euler angle distribution of the particle images for the final 3D reconstructions.

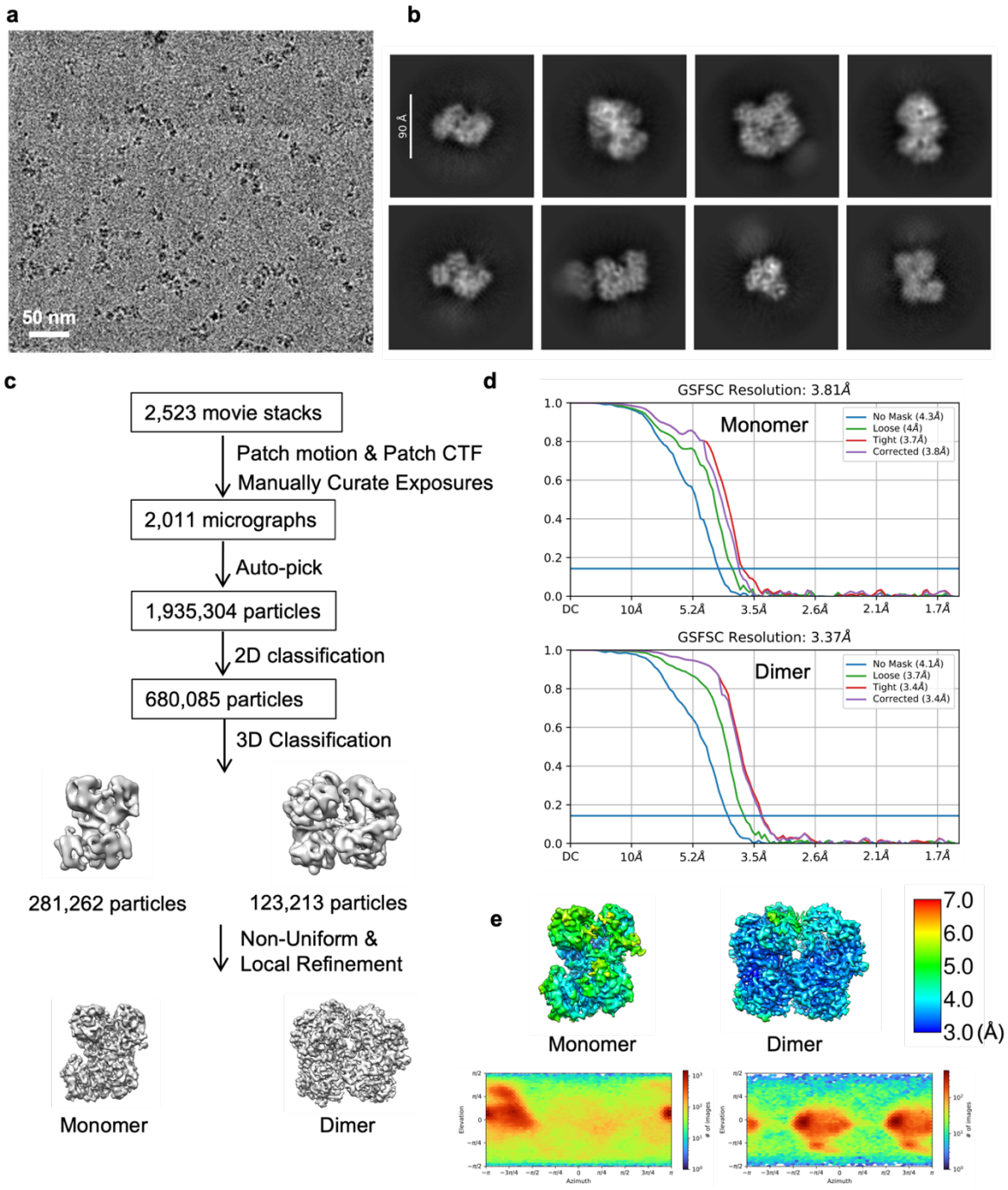

Supplementary Figure 6: Single-particle cryo-EM analysis of the CpAgo-gDNA-tg_ssDNA complex.

a Representative motion-corrected cryo-EM micrograph.

b Reference-free 2D class averages.

c Workflow of the data processing.

d Gold standard FSC plots for the 3D reconstructions, calculated in cryoSPARC.

e Resolution maps and euler angle distribution of the particle images for the final 3D reconstructions.

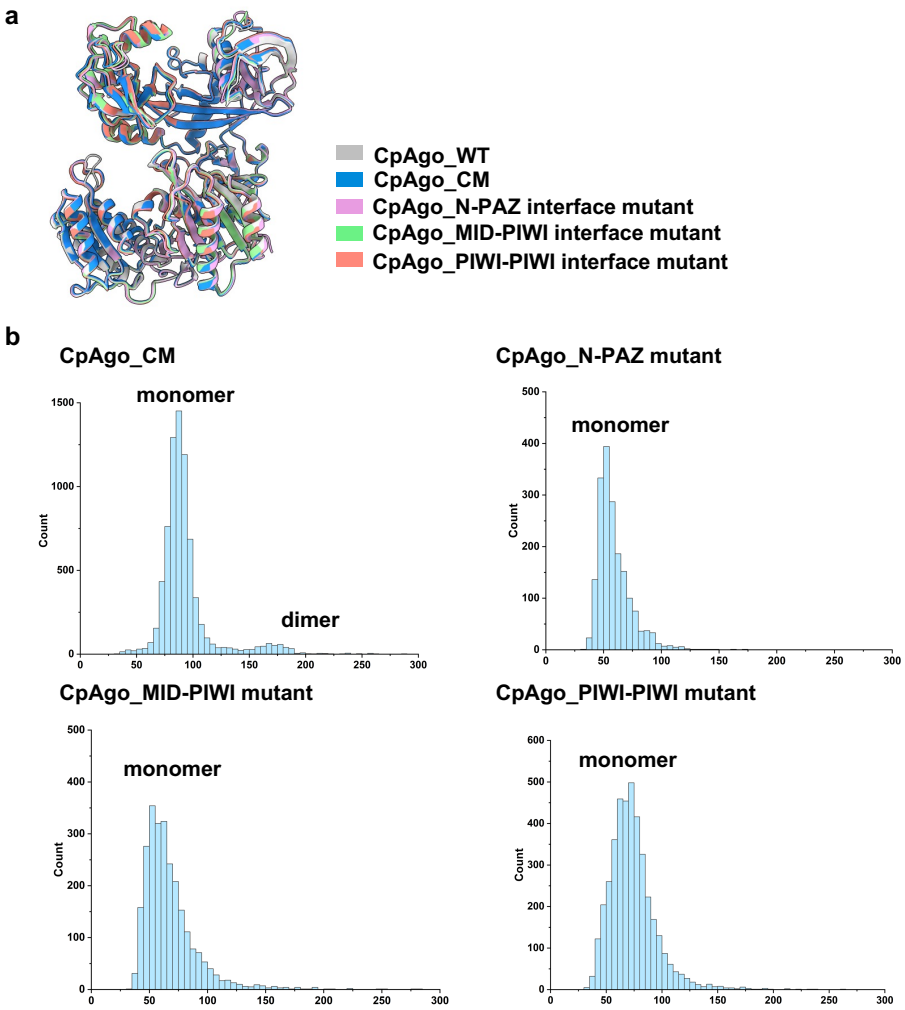

Supplementary Figure 7: Interface mutations disrupt the dimerization of CpAgo.
a The models of CpAgo and its mutants were predicted by AlphaFold3.
b Mass photometry data of CpAgo mutants.

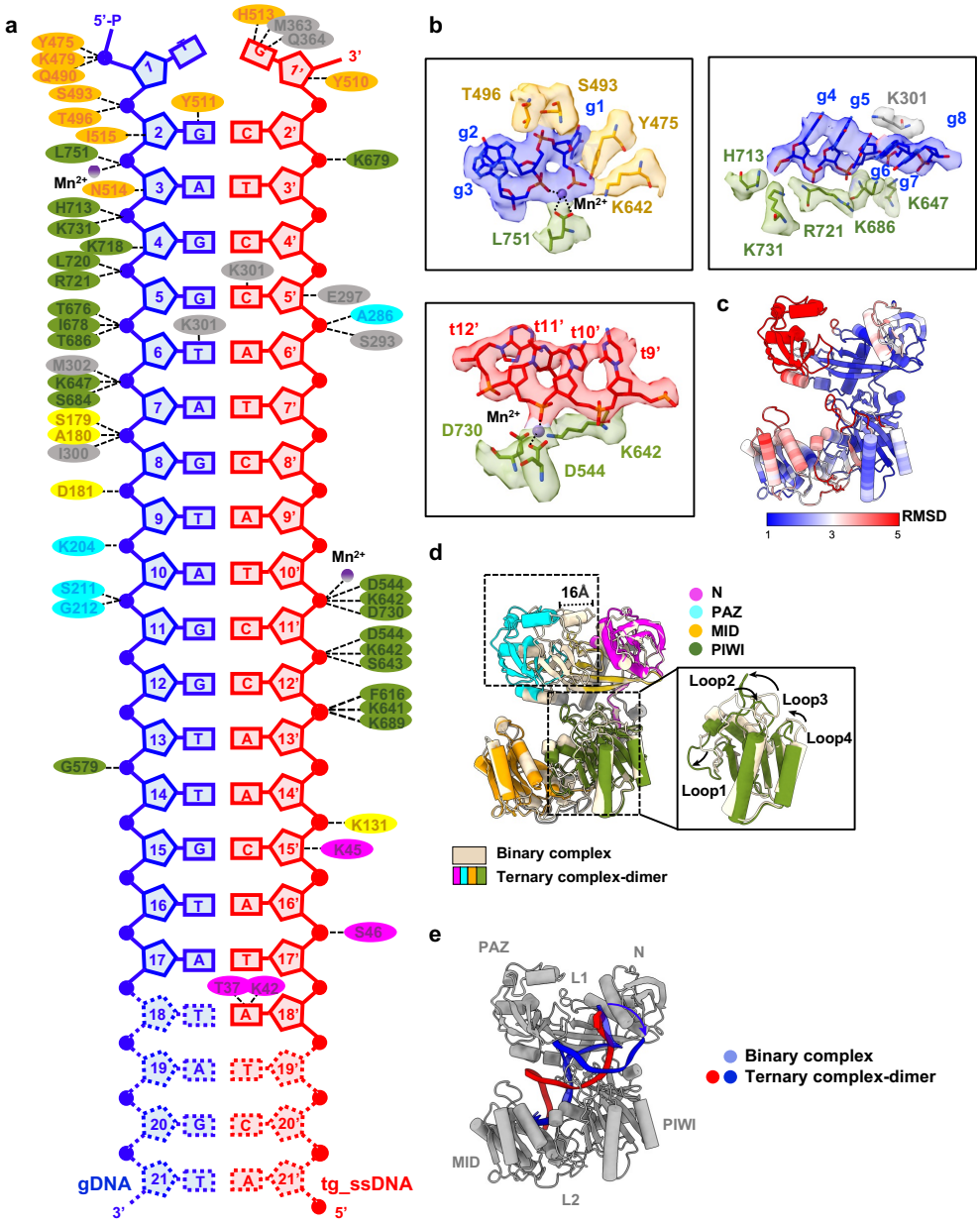

Supplementary Figure 8: Interaction analysis in the dimer structure of the CpAgo-gDNA-tg_ssDNA ternary complex.

a Detailed view of the guide-target DNA duplex in the dimeric form, highlighting key binding points.

b Interaction interfaces between CpAgo and the guide-target duplex in the dimer structure, highlighting key amino acids involved in stabilizing the gDNA and tgDNA.

c Comparison of the ternary complex's dimer unit with the CpAgo-gDNA binary complex, colored by C-alpha RMSD in ChimeraX.

d Comparative structural analysis of the ternary complex's dimer unit and the binary complex, highlighting the shifts in the PAZ and PIWI domains. The movement in PAZ domain and four variable loops of the PIWI domain is marked.

e The nearly 90-degree rotation of the gDNA's 3' end in the dimer structure compared with the binary complex.

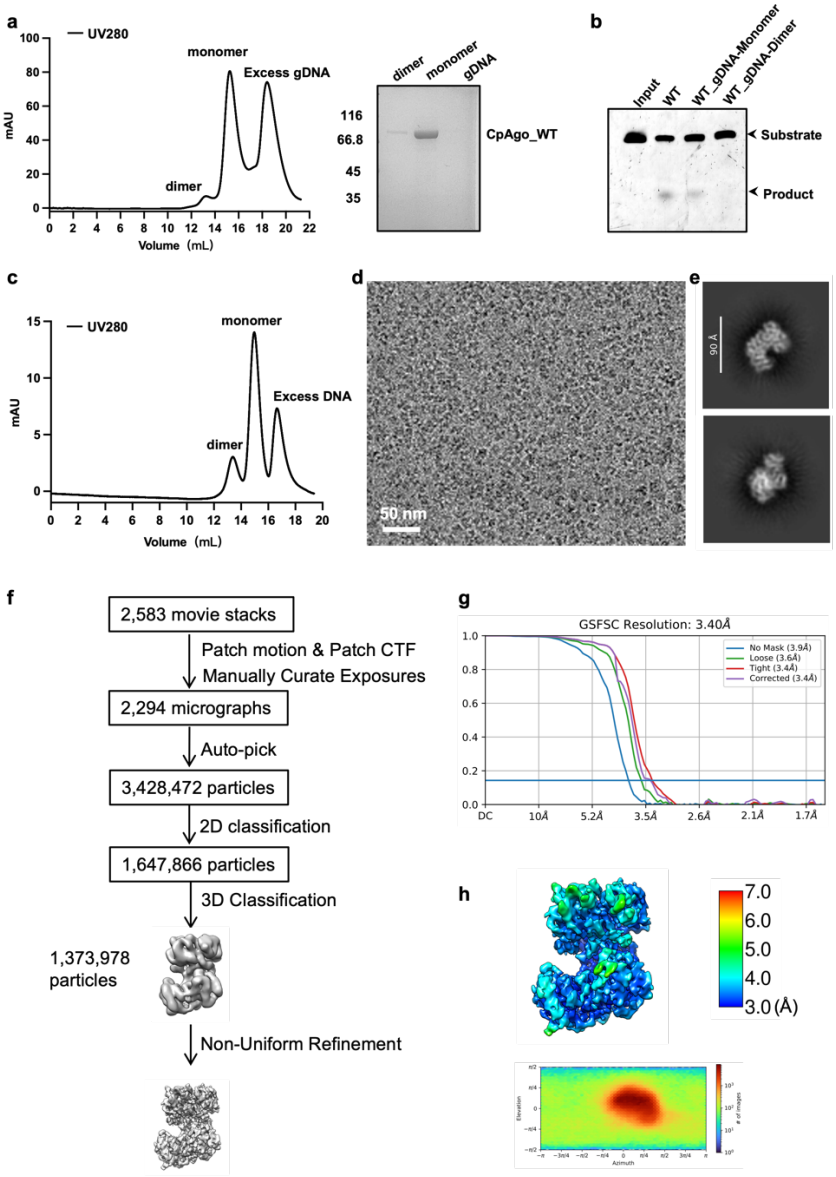

Supplementary Figure 9: Substrate-induced dimerization of CpAgo revealed by SEC and structural analysis.

a SEC profile (left) and SDS-PAGE analysis (right) of CpAgo pre-incubated with gDNA at a 1:2 molar ratio for 20 min.

b tgDNA cleavage assay comparing the catalytic activity of CpAgo-gDNA monomer and dimer fractions.

c SEC profile of ternary complex formation. CpAgo-gDNA monomer was incubated with tg_ssDNA in the presence of Ca^{2+} to prevent cleavage, followed by SEC analysis. A new dimer peak emerged, confirming that functional dimerization is induced upon target engagement.

d Representative motion-corrected cryo-EM micrograph of the CpAgo-gDNA monomer.

e Reference-free 2D class averages.

f Workflow of the data processing.

g Gold standard FSC plots for the 3D reconstruction, calculated in cryoSPARC.

h Resolution map and euler angle distribution of the particle images for the final 3D reconstruction.

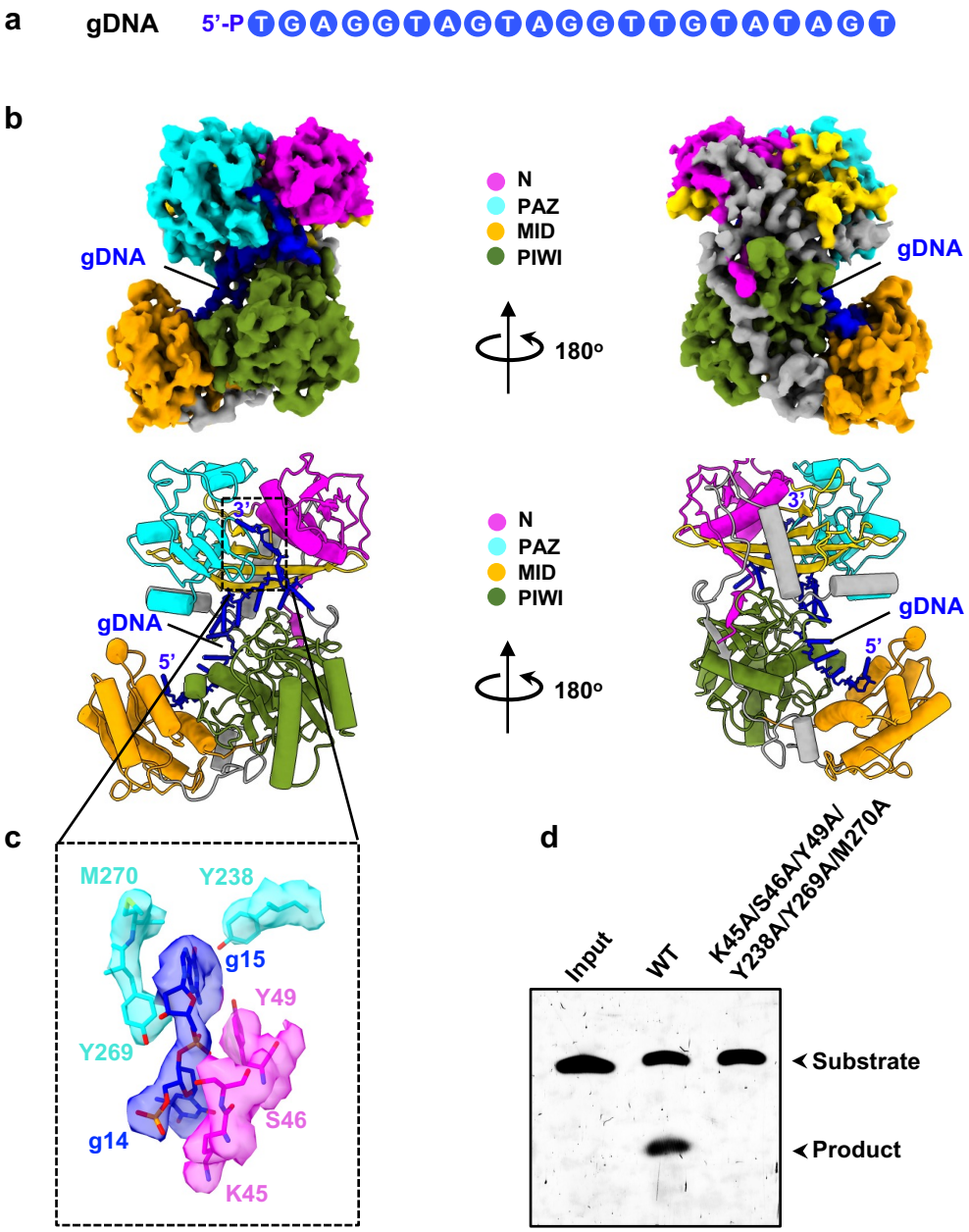

Supplementary Figure 10: Structure of the CpAgo-gDNA monomeric binary complex.
a The schematic for the nucleic-acid sequence used for cryo-EM structural determination of the CpAgo-gDNA binary complex.
b The 3.40-Å cryo-EM map and atomic model of the CpAgo-gDNA binary complex, showing the central cleft where gDNA is positioned.
c Interaction analysis between the gDNA's 3' end and N, PAZ domains, with key anchoring points highlighted.
d Cleavage activity assay results for wild-type (WT) and mutant CpAgo. Mutations disrupting the interactions between the gDNA's 3' end and N, PAZ domains lost their catalytic activity towards tgDNA, indicating that CpAgo adopts a preparatory state upon binding gDNA, poised to recognize the tgDNA.

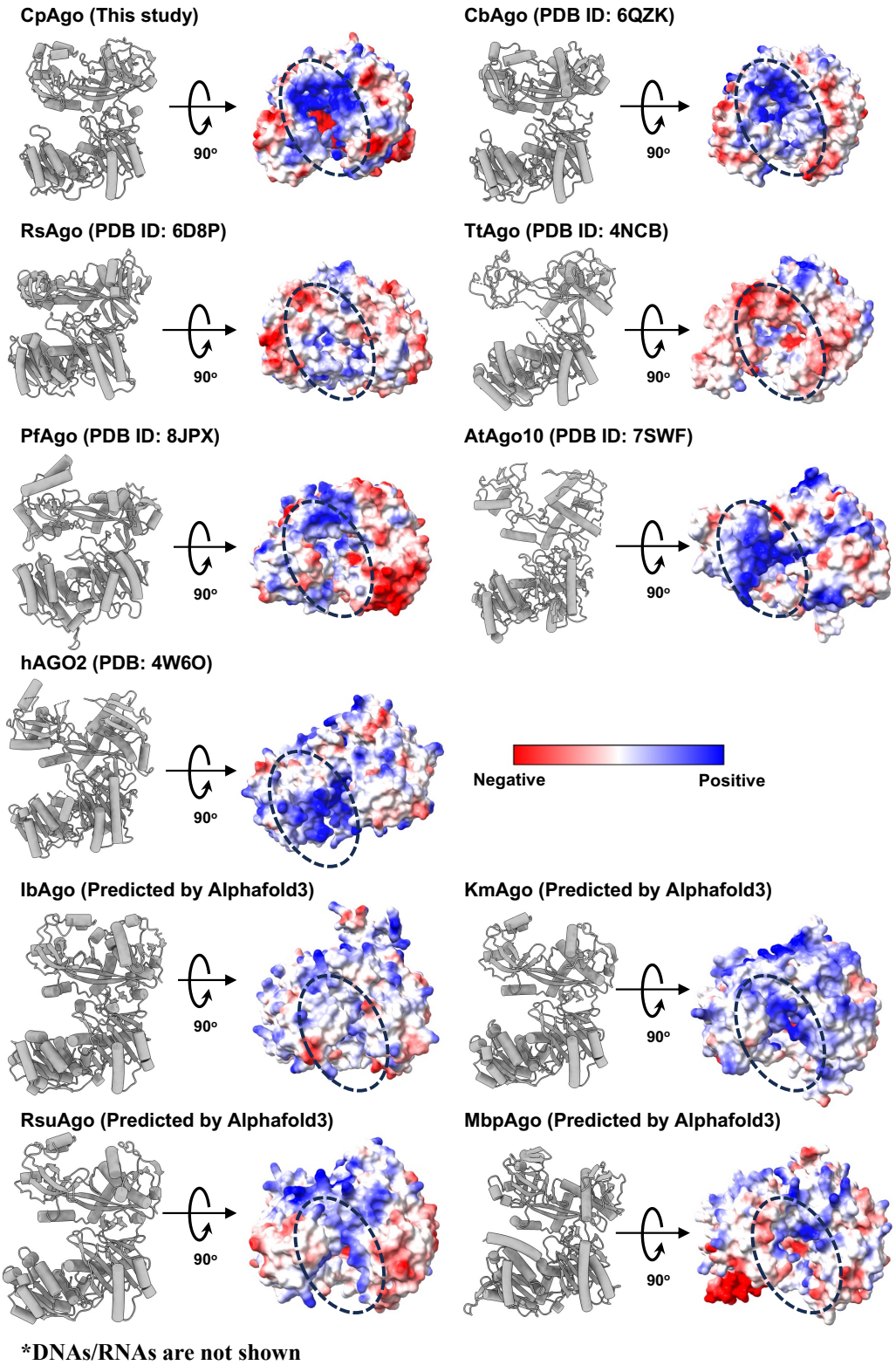

Supplementary Figure 11: The PAZ nucleotide-binding pocket is present in a few Agos. The atomic models of Agos are shown in ribbon, with electrostatic potential analysis shown. The possible PAZ nucleotide-binding pockets in Agos are highlighted in dashed circle.

Supplementary Table 1: Cryo-EM data collection, processing, and model validation of the CpAgo-gDNA-tg_dsDNA complex.

	CpAgo-gDNA-tg_dsDNA	
Data collection and processing		
Microscope	Titan Krios	
Voltage (kV)	300	
Camera	Gatan K3	
Grid type	R2/1 Quantifoil Au grid (200 mesh)	
Magnification	105,000×	
Pixel size (Å)	0.82	
Total exposure ($e^-/Å^2$)	51.064	
Exposure time (s)	2	
Number of frames per exposure	30	
Energy filter slit width (eV)	20	
Data collection software	EPU 2.7	
Number of exposures per hole	5	
Defocus range (μm)	-1.5 to -3.0	
Number of micrographs collected	7175	
Number of micrographs used	6478	
Number of initial particles	8,586,596	
Conformations	Monomer	Dimer
Symmetry	C1	C2
Number of final particles	626,358	820,015
Resolution (0.143 gold standard, Å)	3.42	2.86
Atomic model refinement		
Software	phenix	phenix
Clashscore, all atoms	9.78	5.61
Poor rotamers (%)	0	0
Favored rotamers (%)	97.01	98.05
Ramachandran outliers (%)	0	0
Ramachandran favored (%)	93.81	96.37
MolProbity score	1.92	1.55
Bad bonds (%)	0.02	0
Bad angles (%)	0.05	0
Nucleotide bad bonds (%)	0	0
Nucleotide bad angles (%)	0	0

Supplementary Table 2: Cryo-EM data collection, processing, and model validation of the CpAgo-gDNA-tg_bubble_dsDNA complex.

	CpAgo-gDNA-tg_bubble_dsDNA	
Data collection and processing		
Microscope	Titan Krios	
Voltage (kV)	300	
Camera	Gatan K3	
Grid type	R2/1 Quantifoil Au grid (200 mesh)	
Magnification	105,000×	
Pixel size (Å)	0.82	
Total exposure ($e^-/Å^2$)	48.6	
Exposure time (s)	2.5	
Number of frames per exposure	30	
Energy filter slit width (eV)	20	
Data collection software	EPU 2.7	
Number of exposures per hole	5	
Defocus range (μm)	-1.5 to -3.0	
Number of micrographs collected	2627	
Number of micrographs used	2596	
Number of initial particles	1,609,554	
Conformations	Monomer	Dimer
Symmetry	C1	C2
Number of final particles	159,745	50,418
Resolution (0.143 gold standard, Å)	3.20	3.00
Atomic model refinement		
Software	phenix	phenix
Clashscore, all atoms	11.3	7.46
Poor rotamers (%)	0.15	0.15
Favored rotamers (%)	95.66	97.90
Ramachandran outliers (%)	0.13	0
Ramachandran favored (%)	94.48	95.56
MolProbity score	1.95	1.72
Bad bonds (%)	0	0.02
Bad angles (%)	0.06	0.04
Nucleotide bad bonds (%)	0	0
Nucleotide bad angles (%)	0	0

Supplementary Table 3: Cryo-EM data collection, processing, and model validation of the CpAgo-gDNA-tg_ssDNA complex.

	CpAgo-gDNA-tg_ssDNA	
Data collection and processing		
Microscope	Titan Krios	
Voltage (kV)	300	
Camera	Gatan K3	
Grid type	R2/1 Quantifoil Au grid (200 mesh)	
Magnification	105,000×	
Pixel size (Å)	0.82	
Total exposure ($e^-/Å^2$)	52.44	
Exposure time (s)	2	
Number of frames per exposure	30	
Energy filter slit width (eV)	20	
Data collection software	EPU 2.7	
Number of exposures per hole	5	
Defocus range (μm)	-1.5 to -3.0	
Number of micrographs collected	2523	
Number of micrographs used	2011	
Number of initial particles	1,935,304	
Conformations	Monomer	Dimer
Symmetry	C1	C2
Number of final particles	281,262	123,213
Resolution (0.143 gold standard, Å)	3.81	3.37
Atomic model refinement		
Software	phenix	phenix
Clashscore, all atoms	11.69	5.87
Poor rotamers (%)	0.15	0.15
Favored rotamers (%)	95.96	97.31
Ramachandran outliers (%)	0.13	0
Ramachandran favored (%)	92.46	95.42
MolProbity score	2.05	1.64
Bad bonds (%)	0	0
Bad angles (%)	0.04	0.01
Nucleotide bad bonds (%)	0	0
Nucleotide bad angles (%)	0	0

Supplementary Table 4: Cryo-EM data collection, processing, and model validation of the CpAgo-gDNA complex.

	CpAgo-gDNA
Data collection and processing	
Microscope	Titan Krios
Voltage (kV)	300
Camera	Gatan K3
Grid type	R2/1 Quantifoil Au grid (200 mesh)
Magnification	105,000×
Pixel size (Å)	0.82
Total exposure ($e^-/Å^2$)	47.6
Exposure time (s)	2.5
Number of frames per exposure	30
Energy filter slit width (eV)	20
Data collection software	EPU 2.7
Number of exposures per hole	5
Defocus range (μm)	-1.5 to -3.0
Number of micrographs collected	2583
Number of micrographs used	2294
Number of initial particles	3,428,472
Symmetry	C1
Number of final particles	1,373,978
Resolution (0.143 gold standard, Å)	3.40
Atomic model refinement	
Software	phenix
Clashscore, all atoms	9.96
Poor rotamers (%)	0
Favored rotamers (%)	96.56
Ramachandran outliers (%)	0.13
Ramachandran favored (%)	91.12
MolProbity score	2.04
Bad bonds (%)	0
Bad angles (%)	0.04
Nucleotide bad bonds (%)	0
Nucleotide bad angles (%)	0